ACS APPLIED MATERIALS & INTERFACES

Research Article

www.acsami.org

Nitrogen-Doped Carbon Nanotube Spherical Particles for Supercapacitor Applications: Emulsion-Assisted Compact Packing and Capacitance Enhancement

Donghee Gueon and Jun Hyuk Moon*

Department of Chemical and Biomolecular Engineering, Sogang University, 35 Baekbeom-ro, Mapo-gu, Seoul 121-742, Republic of Korea

Supporting Information

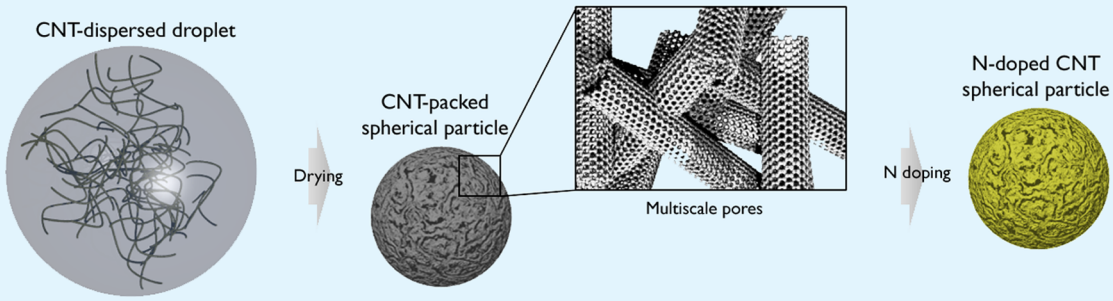

ABSTRACT: The combination of the control of CNT assembly density and the control of intrinsic carbon properties by doping can synergistically improve the supercapacitor performance of CNT-based electrodes. We prepared a dense-packed CNT spherical assembly via emulsion-assisted evaporation and subsequently conducted nitrogen (N) doping to make CNT-based supercapacitors. The assembly of CNT spherical particles is applied as the supercapacitor electrode. We control the N doping content and obtain a specific capacity of 215 F/g at a current density of 0.2 A/g, which is 3.1 times higher than that of the untreated sample. The enhancement stems from high pseudocapacitance and high electrical conductivity that result from the N doping of the CNT assembly. In a comparison of the specific capacitance of N-CNT spherical particles with that of the CNT films prepared by conventional solution-coating, we found that N-CNT samples display a capacitance that is 1.8 times higher, thus confirming the morphological advantage provided by the CNT packing and the hierarchical porous structure in the CNT particle assembly. Our approach allows a facile and high throughput production of high performance electrodes based on CNTs that are commercially available. Moreover, our approach can be extended to produce spherical particles consisting of other nanostructured carbon materials and their composites.

KEYWORDS: *carbon nanotubes, nitrogen doping, droplet confinement, pseudocapacitance, supercapacitors*

INTRODUCTION

Carbon nanotubes (CNTs) are nanostructured carbonaceous materials that are appealing for various energy devices, such as supercapacitors and lithium-ion batteries.[1−3] In addition to their high chemical stability and high electrical conductivity, CNTs have unique morphological characteristics: they possess an intrinsic central canal micropore, and the CNT assembly creates an interconnected meso-to-macroscale pore network among CNTs. These hierarchical porous structures effectively facilitate ion transport in high surface area CNT films and, thus, kinetic properties in their application.[4] However, most CNTs reveal relatively lower energy storage density than other porous carbon materials, including activated carbon and soft- or hard-templated porous carbons.[5,6] In supercapacitor applications, CNT films display the electrochemical capacitance of approximately 100 F/g, while porous carbon materials display a capacitance over 200 F/g.[5,6] One of the reasons for this low capacitance of CNT films is that the dense packing of fibrous CNTs is limited by entanglement. The liquid-evaporation-induced assembly of CNTs has been developed for this purpose. Densely aligned CNTs can be produced by the liquid-induced collapse of vertically aligned CNT arrays.[6,7] Our group utilized the packing of CNTs in a liquid droplet during the evaporation of the solvent.[4]

Meanwhile, the recent improvement of supercapacitance performance in carbon-based electrodes has also been driven by introducing the doping of heteroatoms, such as nitrogen (N)[2,3,8,9] and boron (B).[10] The exact mechanism has not been elucidated, but most of the literature reports that the enhancement of electrochemical capacitance is related to various factors, including the enhancement of electrical conductivity and/or pseudocapacitive properties.[3,9−11] The

Received: June 12, 2015
Accepted: August 24, 2015
Published: September 1, 2015

DOI: 10.1021/acsami.5b05231
ACS Appl. Mater. Interfaces 2015, 7, 20083−20089

Scheme 1. Schematic Procedure of the Fabrication of N-Doped CNT Spherical Particles

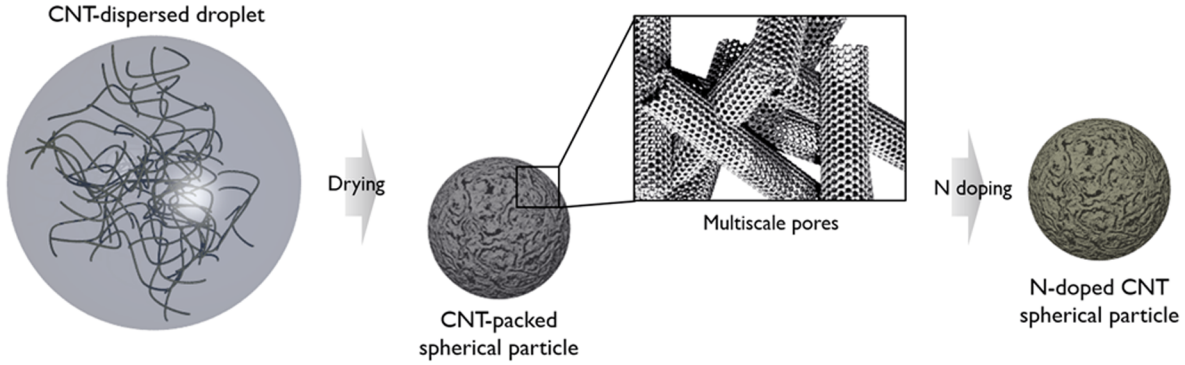

doping enhances the capacitive property of carbon materials even at low doping concentrations. The N doping of graphene-based electrodes produces an increase of capacitance 4 times that of the pristine samples.[12] The N doping of ordered mesoporous carbon yields a capacitance over 200 F/g, which is approximately 2 times higher than that of the untreated sample.[13] However, there have been only a few reports on N-doped CNTs.[3,14] Recently, N-doped CNTs achieved only 60 F/g in their supercapacitor application, which is relatively low compared to other N-doped nanostructured carbon materials.[3] The correlation between doping configuration change and electrical conductivity enhancement has been studied by the heat-treatment of the N-doped CNTs.[15] Thus, combining the control of intrinsic carbon properties by doping and the control of the morphology of CNTs may be a promising approach to obtain synergistic improvement in the capacitance. This approach would also have an impact from the perspective of practical applications of commercially available CNT materials.

Here, we prepare dense-packed CNT assemblies by an emulsion-assisted approach, and subsequently, we conduct N doping for high performance supercapacitor electrodes. Specifically, we control the doping content in the CNT spherical assembly and characterize the doping and its configuration, as well as the doping effect on the electrochemical capacitive properties. We achieve a specific capacitance that is 3.1 times higher with 11.2 at. % N-doped CNT spherical particles, compared to that of the bare CNT spherical particles. The enhancement stems from high pseudocapacitance and high electrical conductivity caused by the N doping of the CNT assembly.[3,9] Moreover, we confirm the morphological advantage of N-doped CNT spherical particles over CNT films in the electrochemical capacitive properties. The CNT spherical particles demonstrate a 1.8 times higher specific capacitance and a higher rate performance, which are attributed to the compact packing of CNTs and the formation of hierarchical porous structures. Our approach is a facile and high throughput method for producing compact packing of CNTs and, simultaneously, multiscale porous morphologies.

EXPERIMENTAL SECTION

Preparation of Carbon Nanotube Spherical Particles and N Doping. An emulsion of an aqueous dispersion of multiwalled carbon nanotubes (CNTs) (Hanhwa Nanotech) in hexadecane is formed by vortex mixing. Here, we add 1 wt % nonionic surfactant (Hypermer 2296, Croda) in the hexadecane. The water inside the droplet was dried in a convection oven at 60 °C overnight, and it left behind CNT spherical assemblies. The CNT assembly particles are rinsed with propylene glycol methyl ether acetate (PGMEA, Aldrich) several times to remove the hexadecane and then heat-treated in a furnace under inert conditions at 500 °C for 2 h to remove residues. For N doping, 1,3,5-triazine-2,4,6- triamine (or melamine) powder (99%, Aldrich) is used as a N source. The mixture of CNT spherical particles and the melamine powder is placed in a tube furnace and treated at 300 °C for 20 min and at 700 °C for 90 min under the N environment.

Electrochemical Measurements. A beaker-type three-electrode system is used to measure the electrochemical properties of the sample. The three-electrode cell is assembled with CNT particle-assembled films on a glassy electrode as a working electrode, a saturated Ag/AgCl electrode (3 M NaCl) as the reference, and a Pt rod as the counter electrode. The mass of CNT particle films was controlled to be 0.35 mg/cm^2. Specifically, the working electrode is prepared by casting a Nafion-added sample solution onto a glassy carbon electrode. We use a 1.0 M H_2SO_4 (Aldrich) solution as an electrolyte solution. Cyclic voltammetry (CV) and galvanostatic charge−discharge curves are measured by VersaSTAT 3 (AMETEK). CV is performed over the voltage range of 0 to 1 V versus Ag/AgCl (3 M NaCl) with a range of scan rates (from 0.01 to 1 V/s). The galvanostatic charge−discharge measurement is measured under a voltage range between 0 and 1 V with a constant current of 0.2−5 A/g.

Characterization. Optical microscopy images of the emulsion were obtained using an optical microscope (Nikon LV100) equipped with a digital camera. Scanning electron microscope images are obtained using a field-emission scanning electron microscope (FESEM, Carl Zeiss, SUPRA 55 VP). Energy-dispersive spectroscopy (EDX, BRUKER, XFlash Detector 4010) elemental mapping is performed to examine the distribution of the N doping. Raman spectra are collected using a Horiba Jobin Yvon LabRAM HR equipped with an air-cooled Ar-ion laser operated at 541 nm. X-ray photoelectron spectroscopy (XPS) is performed using a Leybold spectrometer with an Al Kα monochromatic beam (1486.6 eV) with an input power of 150 W (ESCALAB250 XPS system, Theta Probe XPS system).

RESULTS AND DISCUSSION

The fabrication of N-doped CNT spherical particles is described in Scheme 1. A spherical CNT assembly is achieved by the formation of a CNT aqueous dispersion droplet in hexadecane medium. The evaporation of water by heating the emulsion induces the assembly of CNTs within the spherically confined volume, yielding CNT spherical particles. The capillary pressure exerted by the evaporation of a water droplet enhances the packing of CNTs. Again, the high density of the CNT percolating network enhances the energy density, and the high connectivity among CNTs also increases the conductivity of the CNT assemblies. CNT spherical particles are heat-treated with the presence of melamine under an inert environment. It has been reported that the heat-treatment decomposes the N-rich molecules into carbon nitrides on the carbon matrix.[16,17] Moreover, at higher temperatures, the

DOI: 10.1021/acsami.5b05231
ACS Appl. Mater. Interfaces 2015, 7, 20083−20089

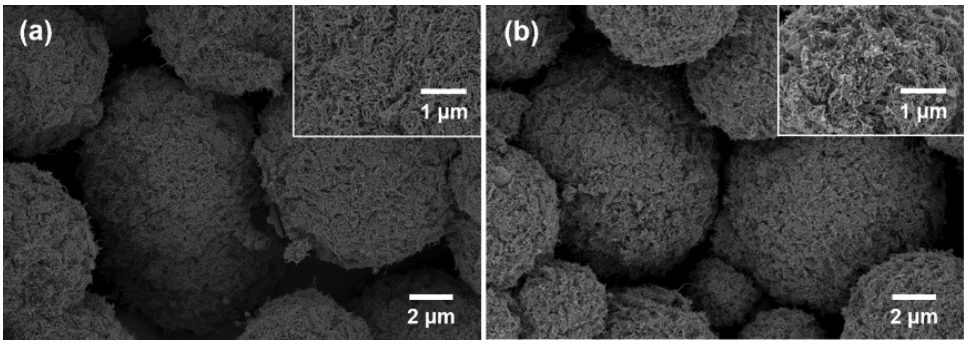

Figure 1. SEM images of (a) bare CNT spherical particles and (b) high-N-doped CNT spherical particles. The insets in parts a and b are the surface images of the respective samples.

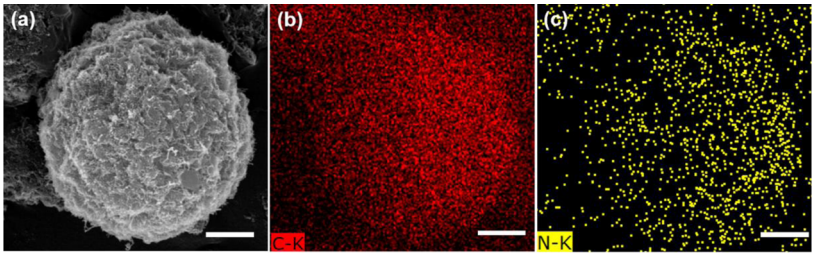

Figure 2. SEM images of (a) high-N-doped CNT spherical particles and the elemental mapping images of (b) carbon and (c) nitrogen (scale bar: 6 μm).

carbon nitrides release the N that diffuses into the carbon matrix.[18] The CNT spherical particles are dispersed in a water−ethanol mixture and coated on the substrate to prepare an electrode film for supercapacitor measurements.

We use a 2 wt % CNT dispersion and prepare a 15.2 ± 4.1 μm sized emulsion droplet, which produces the 9.1 ± 2.3 μm CNT spherical particles after the evaporation, as shown in Figure 1a (see the microscope image of the emulsion droplet and the low magnification SEM image of CNT particles in Figure S1). The N-doped CNT spherical particles have no significant difference in morphology compared to the CNT spherical particles, as displayed in Figure 1b. The BET analysis reveals that the bare and N-doped CNT spherical particles have similar specific area (see Figure S2). The magnified image of the CNT spherical particles in the inset of Figure 1b shows smaller pores and more compact packing of the CNTs relative to the CNT assembly cast on a substrate with evaporation (see Figure S3); the average pore size formed by the CNT mesh is around 20 nm in the CNT spherical particles and around 130 nm in the CNT film. Moreover, it is noted that the CNT spherical particle assembly intrinsically forms macropores of approximately 260 nm among the spherical particles. Here, the N doping concentration is controlled by setting the mixing weight ratio of CNT spherical particles to melamine at 1:200 and 1:600. We designate the samples prepared by using 1:200 and 1:600 mixing ratios as low- and high-N-CNT spherical particles, respectively. The SEM image and the elemental mappings of C and N of single N-doped CNT spherical particles clearly show a uniform doping over the surface (Figure 2a−c).

We measure the Raman spectra of pristine and low- and high-N-CNT spherical particles. The spectra exhibited two peaks at 1350 and 1580 cm^{-1}, which were designated as the D band and the G band, respectively, as shown in Figure 3. The G band is associated with the vibrational modes of the sp^2-bonded

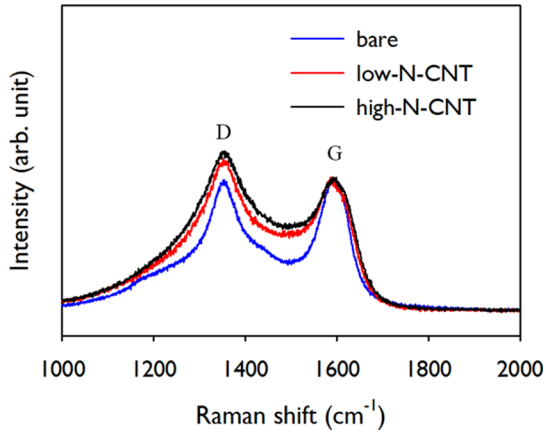

Figure 3. Raman spectra of bare CNT spheres, low-N-doped CNT spheres, and high-N-doped CNT spheres.

carbon atoms in a graphitic layer,[19] whereas the D band is associated with the breathing mode of sp^2-bonding, which appears in disordered graphite.[20] We observed that the N doping enhances the D band intensity. The peak intensity ratio between the D and G bands (I_D/I_G) is 1.01 for the pristine spherical particles and 1.12 and 1.26 for low- and high-N-CNT spherical particles, respectively. This D enhancement implies that the N doping produces a lattice defect in the graphitic layers.

The wide-scan XPS spectra of pristine and low- and high-N-CNT spherical particles display the peaks of C 1s, N 1s, and O 1s as shown in Figure 4. The atomic concentrations of C, N, and O summarized in Table S1 reveal that the low- and high-N-CNT spherical particles have 8.8 at. % and 11.2 at. % of N content, respectively. Moreover, it is observed that, as the N doping increases, the oxygen content is slightly increased. The oxygenated functional groups were often removed by high

DOI: 10.1021/acsami.5b05231
ACS Appl. Mater. Interfaces 2015, 7, 20083−20089

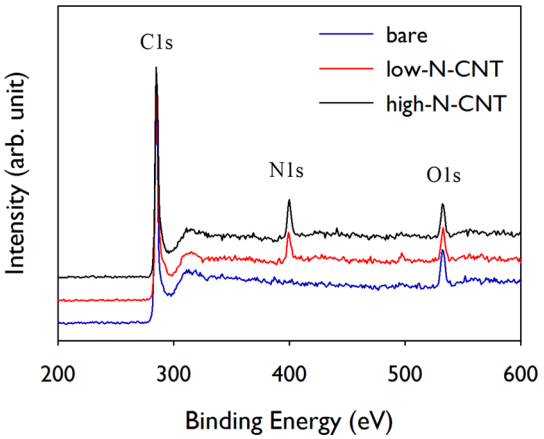

Figure 4. XPS survey spectra of bare CNT spheres, low-N-doped CNT spheres, and high-N-doped CNT spheres.

temperature treatment of the CNTs. Thus, the increase of oxygen content in the doping might imply that the N doping is mediated by the oxygen groups.[17]

The N 1s XPS spectra of low- and high-N-CNT spherical particles, deconvoluted by various N configuration peaks, are displayed in Figure 5a,b, respectively. We use four different configurations of N doping: the pyridinic N (N-6), where the N has an sp^2 hybridization with two C atoms (398.5 eV); the pyrrolic N (N-5), where the N is incorporated into a five-membered ring of C atoms (399.6 eV); the quaternary N (N-Q), where the N has sp^3 hybridized with three C atoms (400.8 eV); and the oxidized N (N-X) group (402.5 eV).[15,21,22] The relative content of these N configurations is compared. The N-CNT spherical particles possess a relatively high portion of the N-6 and N-5 configurations and a low content of the N-Q and N-X configurations as shown in Figure 5c. Previously, as the N doping concentration increased, the concentration ratio of each configuration was maintained.

N-CNT spherical particles are tested as electrodes in a supercapacitor. We prepare the electrode film by assembling N-CNT particles. We observed that the assembled film of CNT spherical particles possesses hierarchical pores of 30 nm at the CNT mesh and 260 nm due to particle packing. The bare CNT spherical particle electrodes are also tested for comparison. We measure the cyclic voltammetry (CV) of bare CNT spherical particles, and it is displayed for low- and high-N-CNT spherical particles at various scan rates. The CV curves of the bare CNT spherical particles have one pair of redox peaks in addition to the double-layer capacitive behavior as shown in Figure 6a. These peaks arise from a faradic redox reaction between quinone and hydroquinone and thus indicate the contribution of the pseudocapacitance.[23] With higher N doping, the CV curve displays a larger current over the potential scan range, i.e., larger capacitance while the quinone–hydroquinone redox peak intensity becomes smaller, as displayed in Figure 6b,c. The capacitance improvement without specific redox peaks by N doping has been explained by the pseudocapacitance obtained by redox reactions at various sites, including the nitrogenated groups or the carbon adjacent to the N atom.[24] Additionally, the increase in the electrical conductivity of CNTs by doping may contribute to the capacitance enhancement, which is confirmed by the voltage drop in the galvanostatic charge–discharge experiment below. As the scan rate increases, the shape of the CV curve is maintained, thus demonstrating fast

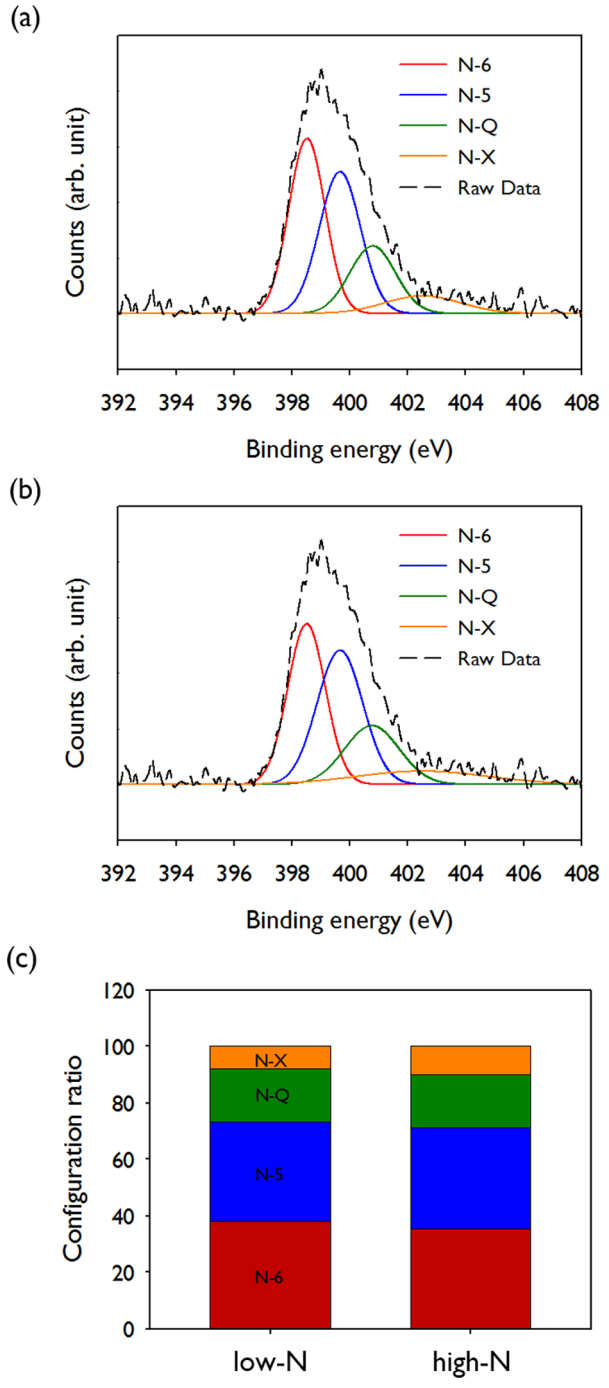

Figure 5. N1 s XPS spectrum (dotted black line) of the (a) low-N-doped CNT spherical particles and (b) high-N-doped CNT spherical particles. The deconvoluted peaks of N-6, N-5, N-Q, and N-X (colored lines) are indicated in each spectrum. (c) The N/C composition ratio for low-N-doped CNT spherical particles and high-N-doped CNT spherical particles.

charge–discharge capability. This result indicates fast electron and ion transfer in the CNT particle-assembled electrodes.

The galvanostatic charge–discharge curves of bare and low- and high-N-CNT spherical particles are measured at various specific current densities as shown in Figure 7a–c, respectively. First, we obtain the ohmic voltage drop in the discharge curve, which corresponds to the resistance of the electrode. The voltage drops for pristine and low- and high-N-CNT spherical particles are 20.6, 6.8, and 3.7 mV, respectively, as noted in each

DOI: 10.1021/acsami.5b05231
ACS Appl. Mater. Interfaces 2015, 7, 20083–20089

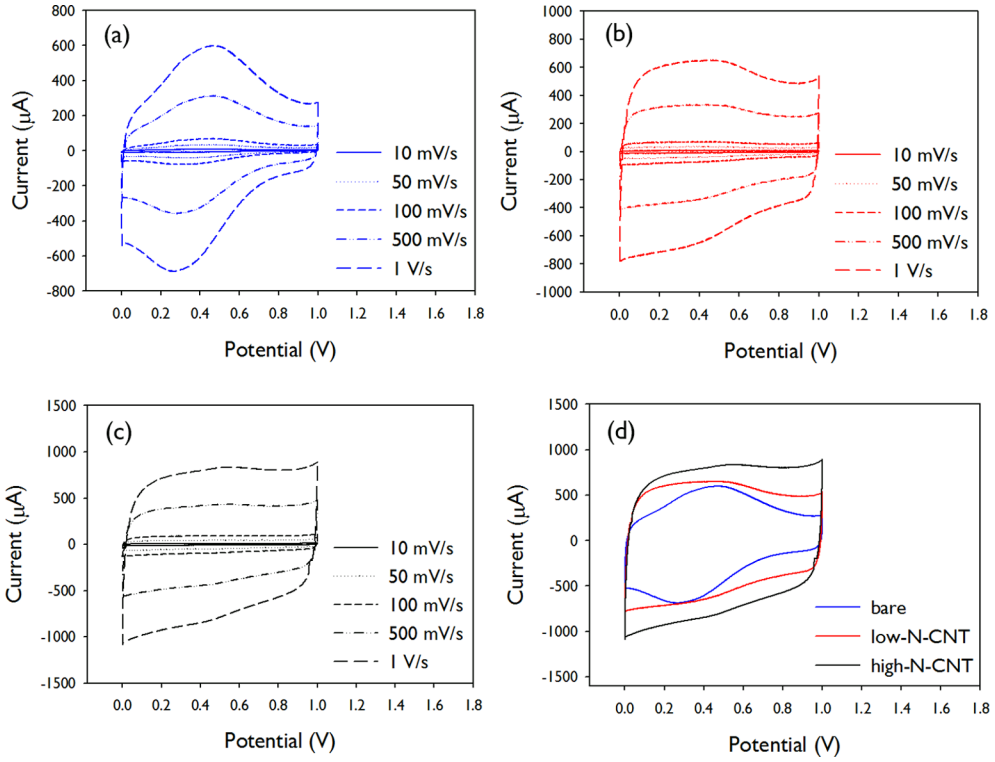

Figure 6. CV curves of (a) bare CNT spherical particles, (b) low-N-CNT spherical particles, and (c) high-N-CNT spherical particles measured at various scan rates from 10 mV/s to 1 V/s in a 1 M H_2SO_4 electrolyte solution. (d) CV curves measured at 1 V/s for bare CNT spherical particles, low-N-CNT spherical particles, and high-N-CNT spherical particles in a 1 M H_2SO_4 electrolyte solution.

figure. Thus, with higher N doping, the electrode resistance becomes smaller.[25] The electrochemical impedance spectroscopy revealed that N doping decreased the charge transfer resistance (see Figure S4). Second, we observe that bare and low- and high-N CNT spherical particles display similar linear charge−discharge profiles at various current densities. Specifically, the profile of high-N CNT spherical particles is more symmetric and linear, which reveals a good capacitive performance. The specific capacitance is calculated from the discharge cycle of a typical voltage−time response curve using the equation[26] $C = (i\Delta t)/(\Delta V m)$, where C is the specific capacitance obtained from the discharge cycle under constant current charge/discharge measurements, i is the constant current, Δt is the discharge time, ΔV is the potential range, and m is the mass of the sample. The specific capacitance at 0.2 A/g of bare and low- and high-N-CNT spherical particles is 69, 128, and 215 F/g, respectively. The cycle performance of high-N-CNT spherical particles evaluated by the measurement of capacitance over charging/discharging cycles reveals >99% over 1500 cycles as shown in Figure S5. Previously, N-doped, activated graphene films have performed approximately 230 F/g at the condition of 0.2 A/g.[27] In the case of N-doped porous graphene-based electrodes, the specific capacitance was 145 F/g.[28] Thus, the N-doped CNT spherical particles display competitive performance compared to that of the graphene-based electrodes.

The capacitance performance of the N-CNT spherical particle film electrode is compared to the N-CNT films prepared by a conventional film casting. We compare the CV measurement of high-N-CNT spherical particles and the N-CNT film at the same scan rate of 500 mV/s, as shown in Figure 8. The area enclosed by the CV cycle, which is proportional to the capacitance of spherical particle electrodes, is approximately 1.8 times larger than that of the film electrode. As we have previously compared by SEM images (Figure 1 and Figure S2), more compact packing and thereby higher density of CNTs in the spherical particles can explain this higher capacitance. Moreover, we compare the specific capacitances of high-N-CNT spherical particles and N-CNT film electrodes at various current densities. Compared to the specific capacitance at 0.2 A/g, the specific capacitance and the current density are 151 F/g (10 times higher) and 38 F/g, respectively. Thus, the capacitance retention is 70% for N-CNT spherical particles and 31% for the N-CNT film. It is observed that the electrode composed of spherical particles yields hierarchical porous structures of mesoscale pores in the spherical particles and also of 260 nm macroscale pores among the particles. Thus, these hierarchical porous electrodes exhibit efficient and fast charge transport properties, which may lead to higher capacitance retention.

CONCLUSIONS

We prepared N-CNT spherical particles that display a high specific capacitance of up to 215 F/g. We induced the compact assembly of CNTs during the evaporation of emulsion droplets and tuned the N doping amount by controlling the amount ratio of N precursor/CNTs during the heat-treatment. We prepared the assembly of N-CNT spherical particles easily by solution-coating of a CNT spherical particle dispersion to produce the supercapacitor electrodes. The 11.2 at. % N-CNT spherical particles achieve a 3 times higher specific capacitance relative to that of the bare CNT spherical particles. This high capacitance of N-CNT spherical particle electrodes is attributed to the enhancement of pseudocapacitance and electrical conductivity, which are caused by the N doping. Moreover,

DOI: 10.1021/acsami.5b05231
ACS Appl. Mater. Interfaces 2015, 7, 20083−20089

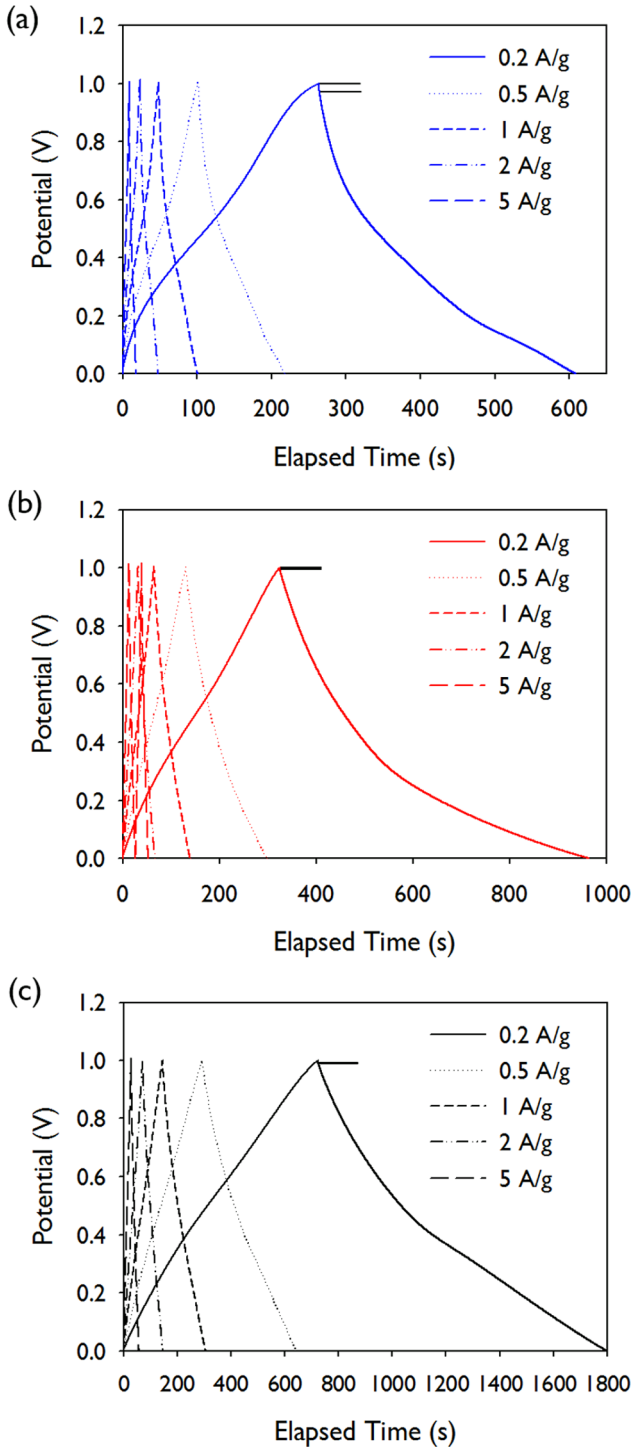

Figure 7. Galvanostatic charge/discharge curves of the (a) bare CNT spherical particles, (b) low-N-CNT spherical particles, and (c) high-N-CNT spherical particles at various current densities from 0.2 to 5 A/g.

the specific capacitance of N-CNT spherical particles produces a 1.8 times higher specific capacitance over conventional CNT films; this result confirms the morphological advantage of the CNT packing and the hierarchical porous structure. Our approach allows a facile and high throughput production of high performance electrodes from CNTs that are commercially available. Moreover, our approach can be extended to produce spherical particles consisting of other nanostructured carbon materials and their composites.

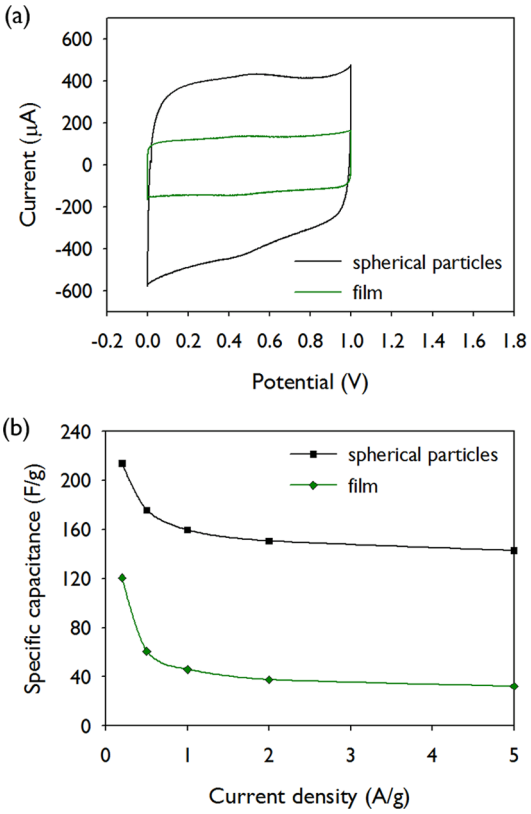

Figure 8. (a) CV curves of the N-doped CNT film and the N-doped CNT spherical particles measured at 500 mV/s in a 1 M H_2SO_4 electrolyte solution. (b) Capacity retention of the N-doped CNT film and the spherical particles at various current densities from 0.2 to 5 A/g.

■ ASSOCIATED CONTENT

Supporting Information

The Supporting Information is available free of charge on the ACS Publications website at DOI: 10.1021/acsami.5b05231.

Additional data including images, isotherms, and atomic compositions (PDF)

■ AUTHOR INFORMATION

Corresponding Author

*E-mail: junhyuk@sogang.ac.kr.

Notes

The authors declare no competing financial interest.

■ ACKNOWLEDGMENTS

This work was supported by grants from the National Research Foundation of Korea (NRF) (Grants 2013R1A1A2010973, 2012M1A2A2671794). The Korea Basic Science Institute is also acknowledged for the SEM and XPS measurements.

■ REFERENCES

(1) Xue, L.; Xu, G.; Li, Y.; Li, S.; Fu, K.; Shi, Q.; Zhang, X. Carbon-Coated Si Nanoparticles Dispersed in Carbon Nanotube Networks as Anode Material for Lithium-Ion Batteries. *ACS Appl. Mater. Interfaces* **2013**, *5* (1), 21−25.

(2) Kim, K.-S.; Park, S.-J. Synthesis and High Electrochemical Capacitance of N-Doped Microporous Carbon/Carbon Nanotubes for Supercapacitor. *J. Electroanal. Chem.* **2012**, *673*, 58−64.

DOI: 10.1021/acsami.5b05231
ACS Appl. Mater. Interfaces 2015, 7, 20083−20089

(3) Sevilla, M.; Yu, L.; Zhao, L.; Ania, C. O.; Titiricic, M.-M. Surface Modification of Cnts with N-Doped Carbon: An Effective Way of Enhancing Their Performance in Supercapacitors. *ACS Sustainable Chem. Eng.* **2014**, *2* (4), 1049−1055.
(4) Kang, D.-Y.; Moon, J. H. Carbon Nanotube Balls and Their Application in Supercapacitors. *ACS Appl. Mater. Interfaces* **2014**, *6* (1), 706−711.
(5) Zhang, J.; Zhang, X.; Zhou, Y.; Guo, S.; Wang, K.; Liang, Z.; Xu, Q. Nitrogen-Doped Hierarchical Porous Carbon Nanowhisker Ensembles on Carbon Nanofiber for High-Performance Supercapacitors. *ACS Sustainable Chem. Eng.* **2014**, *2* (6), 1525−1533.
(6) Zhai, Y.; Dou, Y.; Zhao, D.; Fulvio, P. F.; Mayes, R. T.; Dai, S. Carbon Materials for Chemical Capacitive Energy Storage. *Adv. Mater.* **2011**, *23* (42), 4828−4850.
(7) Xue, L.; Xu, G.; Li, Y.; Li, S.; Fu, K.; Shi, Q.; Zhang, X. Carbon-Coated Si Nanoparticles Dispersed in Carbon Nanotube Networks as Anode Material for Lithium-Ion Batteries. *ACS Appl. Mater. Interfaces* **2013**, *5* (1), 21−25.
(8) Zhang, J.; Zhang, X.; Zhou, Y.; Guo, S.; Wang, K.; Liang, Z.; Xu, Q. Nitrogen-Doped Hierarchical Porous Carbon Nanowhisker Ensembles on Carbon Nanofiber for High-Performance Supercapacitors. *ACS Sustainable Chem. Eng.* **2014**, *2* (6), 1525−1533.
(9) Wickramaratne, N. P.; Xu, J.; Wang, M.; Zhu, L.; Dai, L.; Jaroniec, M. Nitrogen Enriched Porous Carbon Spheres: Attractive Materials for Supercapacitor Electrodes and Co2 Adsorption. *Chem. Mater.* **2014**, *26* (9), 2820−2828.
(10) Han, J.; Zhang, L. L.; Lee, S.; Oh, J.; Lee, K.-S.; Potts, J. R.; Ji, J.; Zhao, X.; Ruoff, R. S.; Park, S. Generation of B-Doped Graphene Nanoplatelets Using a Solution Process and Their Supercapacitor Applications. *ACS Nano* **2013**, *7* (1), 19−26.
(11) Paek, E.; Pak, A. J.; Kweon, K. E.; Hwang, G. S. On the Origin of the Enhanced Supercapacitor Performance of Nitrogen-Doped Graphene. *J. Phys. Chem. C* **2013**, *117* (11), 5610−5616.
(12) Jeong, H. M.; Lee, J. W.; Shin, W. H.; Choi, Y. J.; Shin, H. J.; Kang, J. K.; Choi, J. W. Nitrogen-Doped Graphene for High-Performance Ultracapacitors and the Importance of Nitrogen-Doped Sites at Basal Planes. *Nano Lett.* **2011**, *11* (6), 2472−2477.
(13) Li, M.; Xue, J. Integrated Synthesis of Nitrogen-Doped Mesoporous Carbon from Melamine Resins with Superior Performance in Supercapacitors. *J. Phys. Chem. C* **2014**, *118* (5), 2507−2517.
(14) Wickramaratne, N. P.; Xu, J.; Wang, M.; Zhu, L.; Dai, L.; Jaroniec, M. Nitrogen Enriched Porous Carbon Spheres: Attractive Materials for Supercapacitor Electrodes and Co2 Adsorption. *Chem. Mater.* **2014**, *26* (9), 2820−2828.
(15) Xiao, F.; Song, J.; Gao, H.; Zan, X.; Xu, R.; Duan, H. Coating Graphene Paper with 2d-Assembly of Electrocatalytic Nanoparticles: A Modular Approach toward High-Performance Flexible Electrodes. *ACS Nano* **2012**, *6* (1), 100−110.
(16) Subramanian, N. P.; Li, X.; Nallathambi, V.; Kumaraguru, S. P.; Colon-Mercado, H.; Wu, G.; Lee, J.-W.; Popov, B. N. Nitrogen-Modified Carbon-Based Catalysts for Oxygen Reduction Reaction in Polymer Electrolyte Membrane Fuel Cells. *J. Power Sources* **2009**, *188* (1), 38−44.
(17) Bhattacharjya, D.; Park, H.-Y.; Kim, M.-S.; Choi, H.-S.; Inamdar, S. N.; Yu, J.-S. Nitrogen-Doped Carbon Nanoparticles by Flame Synthesis as Anode Material for Rechargeable Lithium-Ion Batteries. *Langmuir* **2014**, *30* (1), 318−324.
(18) Sheng, Z.-H.; Shao, L.; Chen, J.-J.; Bao, W.-J.; Wang, F.-B.; Xia, X.-H. Catalyst-Free Synthesis of Nitrogen-Doped Graphene Via Thermal Annealing Graphite Oxide with Melamine and Its Excellent Electrocatalysis. *ACS Nano* **2011**, *5* (6), 4350−4358.
(19) Kudin, K. N.; Ozbas, B.; Schniepp, H. C.; Prud'Homme, R. K.; Aksay, I. A.; Car, R. Raman Spectra of Graphite Oxide and Functionalized Graphene Sheets. *Nano Lett.* **2008**, *8* (1), 36−41.
(20) Qian, Y.; Wang, C.; Le, Z.-G. Decorating Graphene Sheets with Pt Nanoparticles Using Sodium Citrate as Reductant. *Appl. Surf. Sci.* **2011**, *257* (24), 10758−10762.
(21) Wang, Z.-L.; Guo, R.; Ding, L.-X.; Tong, Y.-X.; Li, G.-R. Controllable Template-Assisted Electrodeposition of Single-and Multi-Walled Nanotube Arrays for Electrochemical Energy Storage. *Sci. Rep.* **2013**, *3*, 1204.
(22) Hulicova-Jurcakova, D.; Seredych, M.; Lu, G. Q.; Bandosz, T. J. Combined Effect of Nitrogen-and Oxygen-Containing Functional Groups of Microporous Activated Carbon on Its Electrochemical Performance in Supercapacitors. *Adv. Funct. Mater.* **2009**, *19* (3), 438−447.
(23) Andreas, H. A.; Conway, B. E. Examination of the Double-Layer Capacitance of an High Specific-Area C-Cloth Electrode as Titrated from Acidic to Alkaline Phs. *Electrochim. Acta* **2006**, *51* (28), 6510−6520.
(24) Frackowiak, E.; Lota, G.; Machnikowski, J.; Vix-Guterl, C.; Béguin, F. Optimisation of Supercapacitors Using Carbons with Controlled Nanotexture and Nitrogen Content. *Electrochim. Acta* **2006**, *51* (11), 2209−2214.
(25) Fan, Z.; Yan, J.; Wei, T.; Zhi, L.; Ning, G.; Li, T.; Wei, F. Asymmetric Supercapacitors Based on Graphene/Mno2 and Activated Carbon Nanofiber Electrodes with High Power and Energy Density. *Adv. Funct. Mater.* **2011**, *21* (12), 2366−2375.
(26) Zhang, J.; Zhao, X. S. Conducting Polymers Directly Coated on Reduced Graphene Oxide Sheets as High-Performance Supercapacitor Electrodes. *J. Phys. Chem. C* **2012**, *116* (9), 5420−5426.
(27) Wang, P.; He, H. L.; Xu, X. L.; Jin, Y. D. Significantly Enhancing Supercapacitive Performance of Nitrogen-Doped Graphene Nanosheet Electrodes by Phosphoric Acid Activation. *ACS Appl. Mater. Interfaces* **2014**, *6* (3), 1563−1568.
(28) Zheng, C.; Zhou, X. F.; Cao, H. L.; Wang, G. H.; Liu, Z. P. Nitrogen-Doped Porous Graphene-Activated Carbon Composite Derived from "Bucky Gels" for Supercapacitors. *RSC Adv.* **2015**, *5* (14), 10739−10745.

DOI: 10.1021/acsami.5b05231
ACS Appl. Mater. Interfaces 2015, 7, 20083−20089